RSC Advances

PAPER

View Article Online
View Journal | View Issue

Cite this: *RSC Adv.*, 2020, **10**, 23359

Synthesis and characterization of a supported Pd complex on volcanic pumice laminates textured by cellulose for facilitating Suzuki–Miyaura cross-coupling reactions†

Siavash Salek Soltani, [a] Reza Taheri-Ledari, ‡[b] S. Morteza F. Farnia, *[a] Ali Maleki *[b] and Alireza Foroumadi *[cd]

Herein, a novel high-performance heterogeneous catalytic system made of volcanic pumice magnetic particles (VPMP), cellulose (CLS) natural polymeric texture, and palladium nanoparticles (Pd NPs) is presented. The introduced VPMP@CLS-Pd composite has been designed based on the principles of green chemistry, and suitably applied in the Suzuki–Miyaura cross-coupling reactions, as an efficient heterogeneous catalytic system. Concisely, the inherent magnetic property of VPMP (30 emu g^{-1}) provides a great possibility for separation of the catalyst particles from the reaction mixture with great ease. In addition, high heterogeneity and high structural stability are obtained by this composition resulting in remarkable recyclability (ten times successive use). As the main catalytic sites, palladium nanoparticles (Pd NPs) are finely distributed onto the VPMP@CLS structure. To catalyze the Suzuki–Miyaura cross-coupling reactions producing biphenyl pharmaceutical derivatives, the present Pd NPs were reduced from chemical state Pd^{2+} to Pd^{0}. In this regard, a plausible mechanism is submitted in the context as well. As the main result of the performed analytical methods (including FT-IR, EDX, VSM, TGA, FESEM, TEM, BTE, and XPS), it is shown that the spherical-shaped nanoscale Pd particles have been well distributed onto the surfaces of the porous laminate-shaped VPMP. However, the novel designed VPMP@CLS-Pd catalyst is used for facilitating the synthetic reactions of biphenyls, and high reaction yields (~98%) are obtained in a short reaction time (10 min) by using a small amount of catalytic system (0.01 g), under mild conditions (room temperature).

Received 21st May 2020
Accepted 15th June 2020

DOI: 10.1039/d0ra04521g

rsc.li/rsc-advances

1. Introduction

In the field of organic catalysis, designing novel heterogeneous catalytic systems in micro and nano scales has attracted so much attention by researchers, in the last couple of decades.[1–3] This is due to high facilities in the complex synthetic processes provided by nanocatalysts and effective chemical interactions between the involved reactants and the catalytic substrate. Among all of the heterogeneous catalytic species, magnetic systems have been more applied due to high ease in further purification processes.[4] Previously, we have reported several magnetic systems based on iron oxide nanoparticles, as the magnetic core for catalytic and drug delivery purposes.[5–11] The most important point in application of the magnetic systems, which show magnetic saturation above 10 emu g^{-1} in magnetic–hysteresis curves,[5,12] is a convenient separation process after completion of the reaction. This is performed just by holding an external magnet at the bottom of the reaction flask and decanting the content. In this regard, so many nano- and micro-scaled composites have been designed and introduced for catalytic purposes, in which various types of organic and inorganic materials are used.[13–15] Briefly, the magnetic materials are commonly used for the convenient separation processes, and the main catalytic active sites are provided by other components such as organic structures, polymers, inorganic particles, biological structures *etc.* For instance, the surface of the magnetic core has been modified by a polymer, and silver NPs were added and used as the main catalytic site.[16] In the same way, different shells have been considered for core coating such as silica,[17] calcium carbonate,[18] copper

[a]*School of Chemistry, College of Science, University of Tehran, Tehran, Iran. E-mail: mfarnia@khayam.ut.ac.ir; Tel: +98 2166495291*

[b]*Catalysts and Organic Synthesis Research Laboratory, Department of Chemistry, Iran University of Science and Technology, Tehran 16846-13114, Iran. E-mail: maleki@iust.ac.ir; Fax: +98-21-73021584; Tel: +98-21-77240540-50*

[c]*Drug Design and Development Research Center, The Institute of Pharmaceutical Sciences (TIPS), Tehran University of Medical Sciences, Tehran, Iran. E-mail: aforoumadi@yahoo.com; Tel: +98 2166954708*

[d]*Department of Medicinal Chemistry, Faculty of Pharmacy, Tehran University of Medical Sciences, Tehran, Iran*

† Electronic supplementary information (ESI) available: H NMR spectra of the selected products. See DOI: 10.1039/d0ra04521g

‡ Co-first author.

nanoparticles,[19] palladium nanoparticles,[20] and *etc.* Recently, researchers have tried to design some novel heterogeneous catalytic systems by employing the natural bases, in accordance with the principles of the green chemistry.[21,22] Since, biocompatibility is another important point that has attracted so much attentions in the last years. In this regard, various natural species such as clays[23] and polymers[24] have been exploited. One of the inherently magnetic natural materials is volcanic pumice that includes highly porous structure.[25–27] Previously, we used that as a substantial basis for the preparation of the efficient catalytic systems due to its high magnetic property, biocompatibility, great surface functionalization capability, and mesoporous structure.[28,29] Herein, we use well grinded volcanic pumice as the natural basis for another novel catalytic system.

As a substantial polymeric substrate with a biocompatible origin, cellulose (CLS) has been considered due to its featured features. As the first property from chemical aspect, there are numerous hydroxyl groups (–OH) onto the CLS strands that provide suitable chemically active sites for covalent bindings and well composition with pumice particles through physicochemical H-bindings.[29–32] From the other side, these active –OH functional groups are appropriate for chelation by cationic metals such as copper[33] and palladium.[34] From mechanical aspect, composition of the CLS textures with other inorganic components forms a stable hybrid structure that is considered as an important factor in the architecture of the heterogeneous catalytic systems. Moreover, from the environmental aspect, the existence of this natural ingredient significantly increases biocompatibility of the catalytic systems, and make the catalytic systems more suitable for scaling up and industrial applications. In this regard, in this work, we have tried to make an instrumental composition between volcanic pumice magnetic particles (VPMP) and CLS as the main inorganic and organic natural bases, respectively. Then, palladium nanoparticles (Pd NPs) are added to the system, as the main catalytic active sites. Reportedly, Pd NPs have been successfully used in C–C coupling reactions in the composition form with other materials and in nano scale.[35] For instance, we have executed this approach by using poly 4-vinylpyridine polymeric substrate and iron oxide magnetic nanoparticles.[36]

Biphenyls, as one of the most important pharmaceutical compounds are synthesized *via* C–C coupling approach.[37] The use of various biphenyl derivatives in cancer therapy,[38] arteriosclerosis,[39] osteolytic disorders, ophthalmic disorders, and their use as integrin antagonists,[40] lead researchers to introduce novel convenient synthetic methods for them. Meanwhile, designing novel catalytic systems including Pd NPs has found great importance and attracted so much attentions because Pd plays a key role in C–C couplings.[35,41,42] In this regard, we intend to introduce a novel designed Pd-containing catalytic system for the convenient synthesis of biphenyl derivatives.

Herein, a novel method for the convenient and fast synthesis of biphenyl derivatives by using a novel designed catalytic system made of natural VPMP and CLS, and also Pd NPs is presented. This VPMP@CLS-Pd catalyst is easily separated from the reaction mixture through its magnetic property, and could be reused for several times due to its substantial recyclability. However, obtaining high reaction yields for biphenyl derivatives (*ca.* 98%) during a fast catalytic process (10 min) under mild conditions, well highlight the advantages of the presented VPMP@CLS-Pd natural based nanocomposite for the catalytic applications. In this work, we monitor the catalytic activity of both as-prepared VPMP@CLS-Pd(0) catalyst and freshly prepared version (in which Pd(II) NPs are recused during an *in situ* process), as well.

2. Results and discussion

2.1. Preparation of VPMP@CLS-Pd nanocatalyst

Fig. 1 schematically presents the preparation route of desired VPMP@CLS-Pd composite. Accordingly, the purchased pumice powder was grinded *via* ball-milling to produce the uniform particles. Then, to deplete the pores of the pumice plates from useless fillers, calcination process was performed at high temperature in a furnace. After confirming the uniformity and successful separation of the pumice plates from the filler by electron microscopy (EM), a portion of the pumice powder was dispersed in a concentrated solution of CLS (*via* ultrasonication) and mixed at mild conditions. After completion of the process, the particles were magnetically segregated and washed to remove the excess unbonded CLS. Since, there are numerous –OH functional groups in the structures of VPMP and CLS, so many physicochemical H-bindings are formed during the mixing process.[29,32] So, a stable composite is created, which can be used for several times. Afterward, palladium chloride salt was dissolved in a separate flask in a hot acidic medium and cooled down after resulting a red clear solution. The –OH groups of the as-prepared heterogeneous VPMP@CLS were activated in an alkaline aqueous solution in another flask. Next, the prepared palladium solution was added to the dispersed mixture of VPMP@CLS during the stirring. In order to have well distribution of Pd NPs onto the VPMP@CLS particles, the addition of palladium solution was performed drop by drop. After completion of the reaction, the formed light brown powder were magnetically separated and well washed to remove excess salts and ions that are entrapped into the pores and silica network of VPMP. The appearance and change in the color of the heterogeneous particles is also illustrated in Fig. 1. Ultimately, the composed Pd NPs onto the surfaces were reduced to Pd(0) by sodium borohydride in the presence of triphenylphosphie that act as a reducing agent and ligand for Pd(II), respectively. Herein, we intended to monitor the catalytic activity of both as-prepared VPMP@CLS-Pd(0) system, in which Pd^0 is obtained from Pd^{2+} in the final stage of the preparation route (according to Fig. 1), and the freshly prepared version in which VPMP@CLS-Pd(II) is added to the reactants of Suzuki–Miyaura and the combined Pd nanoparticles (in chemical state 2+) are simultaneously reduced during an *in situ* process. In the practical sections, we found out that using the freshly prepared VPMP@CLS-Pd(0) results in higher efficiency. Hence, VPMP@CLS-Pd(II) and related materials for reduction of Pd^{2+} (including PPh_3, $NaBH_4$, and Ca_2CO_3) are added to the coupling reaction's components (see the Experimental section). As a probable reason, it could be expressed that the Pd

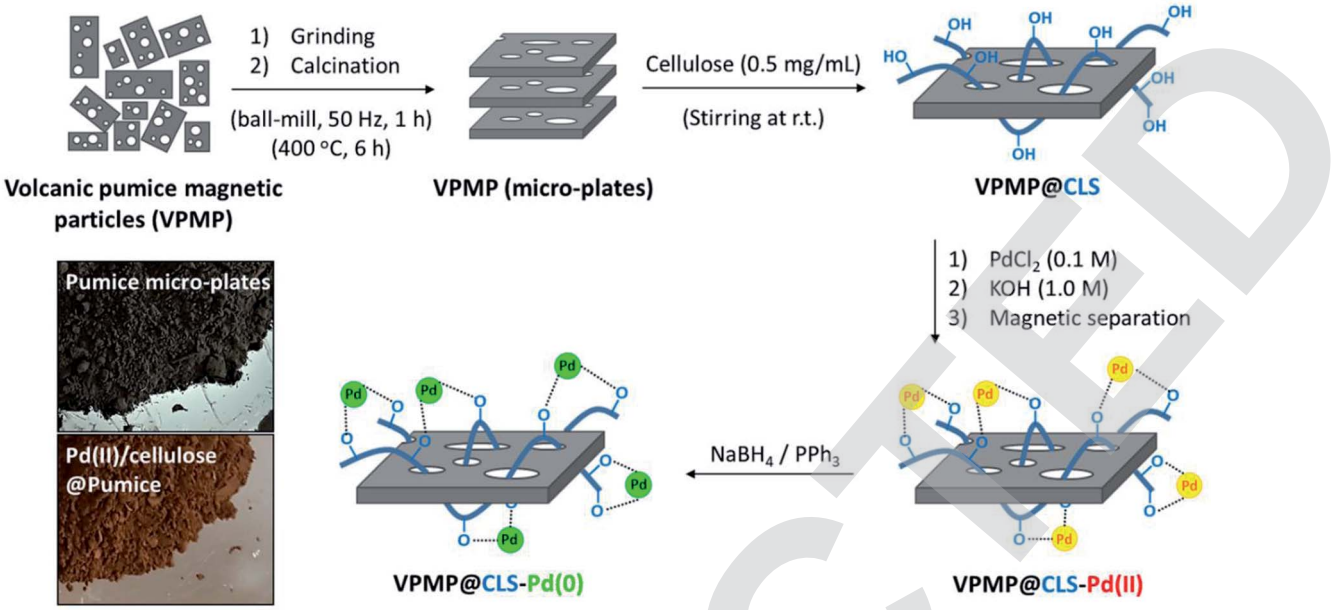

Fig. 1 Step by step preparation pathway for VPMP@CLS-Pd catalytic system.

nanoparticles in chemical state (0) are not so stable on the VPMP, at the storage conditions. Since, the silica network present in the structure of VPMP acts as a great molecular sieve, an oxidation process may be occurred by the entrapped moisture (water and oxygen) into the silica network on the reduced Pd nanoparticles. The obtained results from the mentioned experiments are reported in Table 1 (entries 5 and 6), in the optimization section.

2.2. Characterization of VPMP@CLS-Pd nanocatalyst

As the first method for characterization, Fourier-transform infrared (FT-IR) spectra of the neat pumice powder (before and after the calcination process), VPMP@CLS binary hybrid, and VPMP@CLS-Pd composite were prepared and investigated. It should be noted that all of the characterization analyses have been done on VPMP@CLS-Pd(0) sample (not Pd^{2+}). As can be seen in Fig. 2(a), the peak intensity at 1000–1200 and 3450 cm^{-1} that are related to stretching vibrations of O–H bonds and bending vibrations of Si–O–Si bonds, respectively, has been significantly increased after performing the calcination process. This is likely due to removing the fillers from the interior spaces of the VPMP and getting cleaner structure by silica network. In addition, the peaks related to Si–OH and SiO–H bands have been appeared at *ca.* 900 and 800 cm^{-1}, respectively, after the calcination process. In the spectrum related to VPMP@CLS, the appearance of a keen peak at *ca.* 2900 cm^{-1} proves the existence of CLS in the structure. This peak coming from the stretching vibrations of C–H bonds with hybridation state sp^3. Ultimately, a peak emerged at *ca.* 1550 cm^{-1} shows that there are also a numbers of PdO NPs in the structure of the catalyst, even after performing the reduction process.[43] However, to obtain more confirmation on the existence of the essential elements, energy-dispersive X-ray (EDX) spectroscopy was considered. As can be observed in Fig. 2(b and c), a comparison was made between the fabricated VPMP@CLS-Pd and the neat VPMP showing that the peak intensity of carbon element has been significantly increased and this is attributed to well composition of CLS with VPMP. Also, it has been clearly demonstrated that 3.5 wt% of the total weight of the fabricated VPMP@CLS-Pd belongs to the Pd NPs.

As discussed in the introduction section, VPMP@CLS-Pd particles could be conveniently separated after completion of the synthetic reactions from reaction mixture. This is carried out just by using an external magnet at the bottom of the flask and decanting the content. In this regard, vibrating-sample

Table 1 Optimization of the reaction conditions for the synthesis of biphenyl from 4-nitroiodobenzene and phenylboronic acid, using VPMP@CLS-Pd catalytic system

Entry	Medium	Temperature (°C)	Catalyst (g)	Time (min)	Yield[a] (%)
1	Water	25	0.01	10	Trace
2	Water/EtOH	25	0.01	10	68
3	DMF	25	0.01	10	94
4	DMSO	25	0.01	10	96
5	DMSO	25	0.01	10	98[b]
6	DMSO	25	0.01	10	94[c]
7	DMSO	60	0.01	10	98
8	DMSO	25	0.02	10	98
9	DMSO	25	0.01	30	98

[a] Isolated yields, 4-iodonitrobenzene (1.0 mmol) and phenylboronic acid (1.2 mmol), in the presence of $NaBH_4$ (0.1 mmol), K_2CO_3 (1.5 mmol), PPh_3 (0.1 mmol, 0.0026 g), and the solvent (5.0 mL), under inert atmosphere. [b] Optimum conditions: in which VPMP@CLS-Pd(II) catalyst was used under reduction conditions. [c] As-prepared VPMP@CLS-Pd(0) was used in the absence of PPh_3, $NaBH_4$, and K_2CO_3.

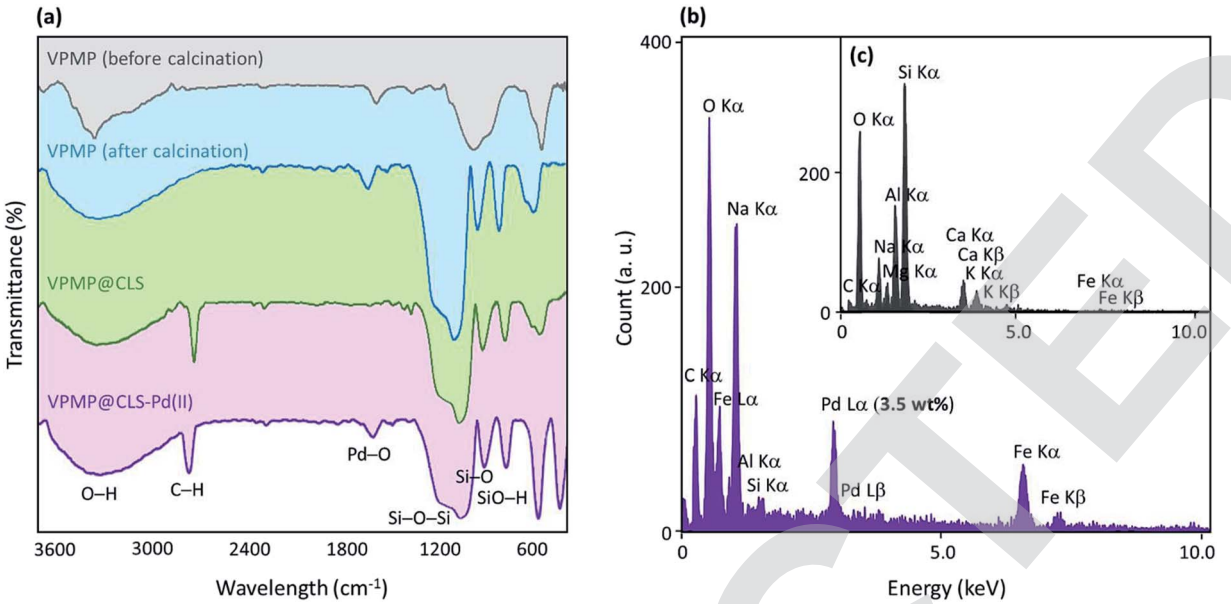

Fig. 2 (a) FT-IR spectra of the neat VPMP (before and after the calcination process), VPMP@CLS binary composite, and VPMP@CLS-Pd catalyst, and (b and c) EDX spectra of the fabricated VPMP@CLS-Pd catalyst and the neat VPMP, respectively.

magnetometer (VSM) analysis was performed to show great magnetic behavior of the natural particles. As Fig. 3(a) exhibits, this substantial physical property inherently exists in the VPMP. According to the figure, magnetic hysteresis (*M–H*) curve of the neat VPMP (Fig. 3(a), red curve) has been saturated at *ca.* 45 emu g^{-1}, whereas this value has been reduced to *ca.* 30 emu g^{-1} (black curve). Obviously, the magnetic property of an individual magnetic component is decreased through composition and mixing with some non-magnetic ingredients. However, this amount of magnetic saturation for the VPMP@CLS-Pd system well proves that they are able to be magnetically separated, recycled, and reused again.[14,19]

Thermal decomposition of the fabricated VPMP@CLS-Pd system was also compared with the neat VPMP by thermogravimetric analysis (TGA). According to the curves shown in Fig. 3(b), the main difference between two curves is clearly observed where *ca.* 35% weight lost in a range of 210–590 °C is occurred for VPMP@CLS-Pd (black curve), whereas only *ca.* 7% has been occurred for the neat VPMP till around 500 °C (red curve). In the TGA curve of VPMP@CLS-Pd, this huge weight lost coming from the removal of –OH groups present in the

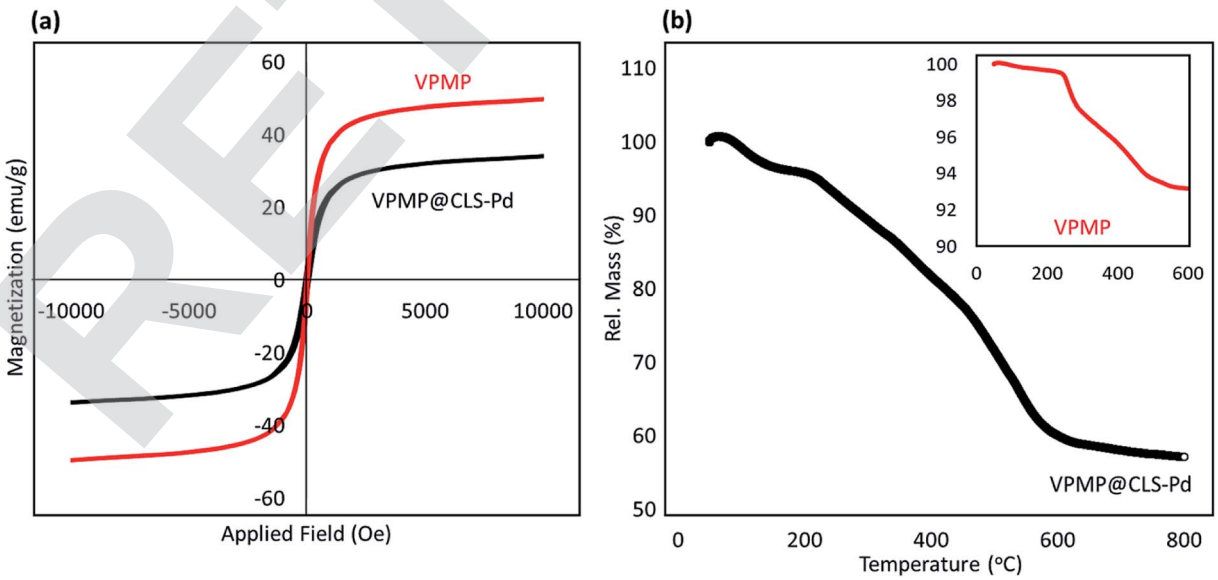

Fig. 3 (a) Room temperature *M–H* curves, and (b) TGA curves of the sole VPMP (red color) and the fabricated VPMP@CLS-Pd composite (black color).

structure of the CLS. According to literature, the –OH groups of polymers leave the structure during dehydration process at this thermal range.[44] Above 600 °C, Pd and VPMP NPs start to decomposition where a gradual weight lost is observed in the curve. In the TGA curve of the neat VPMP (red curve), *ca.* 7% weight lost is likely related to the removal of the entrapped water molecules from the silica network of VPMP. Since, the silica network acts as a great molecular sieve, there is a great capacity at the VPMP structure for water trapping.[6,8,17] In both TGA curves, the first shoulder is related to the separation of physically adsorbed moisture onto the surfaces, which are removed by heating to around 200 °C. These amounts are *ca.* 5 and 1 wt% for VPMP@CLS-Pd and sole VPMP, respectively. As a logical justification, jelly nature of CLS polymer causes to adsorb more volumes of the moisture in the air.

To investigate morphology, size, and composition attitude of the used ingredients, field-emission scanning electron microscopy (FESEM) and transmission electron microscopy (TEM) were performed on the samples. As Fig. 4(a) illustrates, micro-sized plates of VPMP have been well dispersed and separated from each other after grinding *via* ball-milling. Before it, they are so agglomerated that are not suitable for doing the composition process at this attitude. Fig. 4(b) demonstrates the composition attitude of the CLS strands with Pd NPs, which have been appeared as the spherical particles with high uniformity. Image (c) shows these spherical particles in more magnification. As indicated in the image (c), size distribution of the formed Pd NPs is in a size range of 50–150 nm and the mean size was estimated (by Digimizer software) in *ca.* 89 nm diameter. Size distribution diagram of the formed particles has been given in ESI files (Fig. S11†). Finally, TEM imaging (Fig. 4(d)) has revealed that the Pd NPs (dark spots in the image) have been well distributed onto the VPMP surfaces (light plates), during the composition process.

As claimed in the introduction section, the mesoporous structure of VPMP leads to obtain high reaction yields for the synthesized biphenyl derivatives because nanoscale pore sizes are able to capture the molecules of the reactants and make them more available for each other. To investigate physisorption isotherms of the porous structure of VPMP@CLS-Pd composite, Brunauer–Emmett–Teller (BET) surface area analysis was carried out on the neat VPMP and VPMP@CLS-Pd composite samples, *via* adsorption/desorption of N_2 gas (Fig. 5(a)). The relatively reversible isotherm of the neat VPMP is a typical type II, which is related to macroporous materials. The prepared VPMP@CLS-Pd composite has shown the type IV isotherm of mesoporous materials (pore size 2–50 nm) with a hysteretic loop in the range from 0.6 to 0.9 P/P_0. As expected,

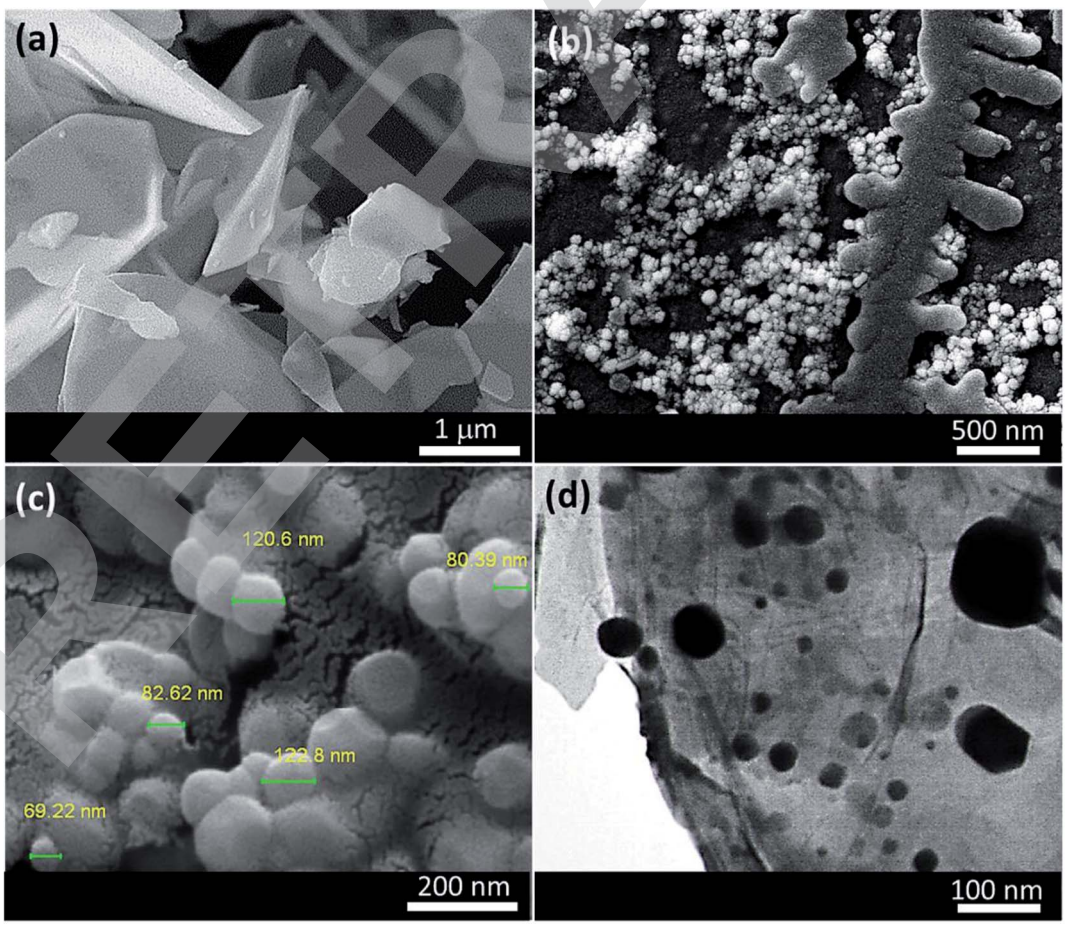

Fig. 4 FESEM images of (a) neat grinded VPMP, (b and c) the fabricated VPMP@CLS-Pd composite, and (d) TEM image of VPMP@CLS-Pd.

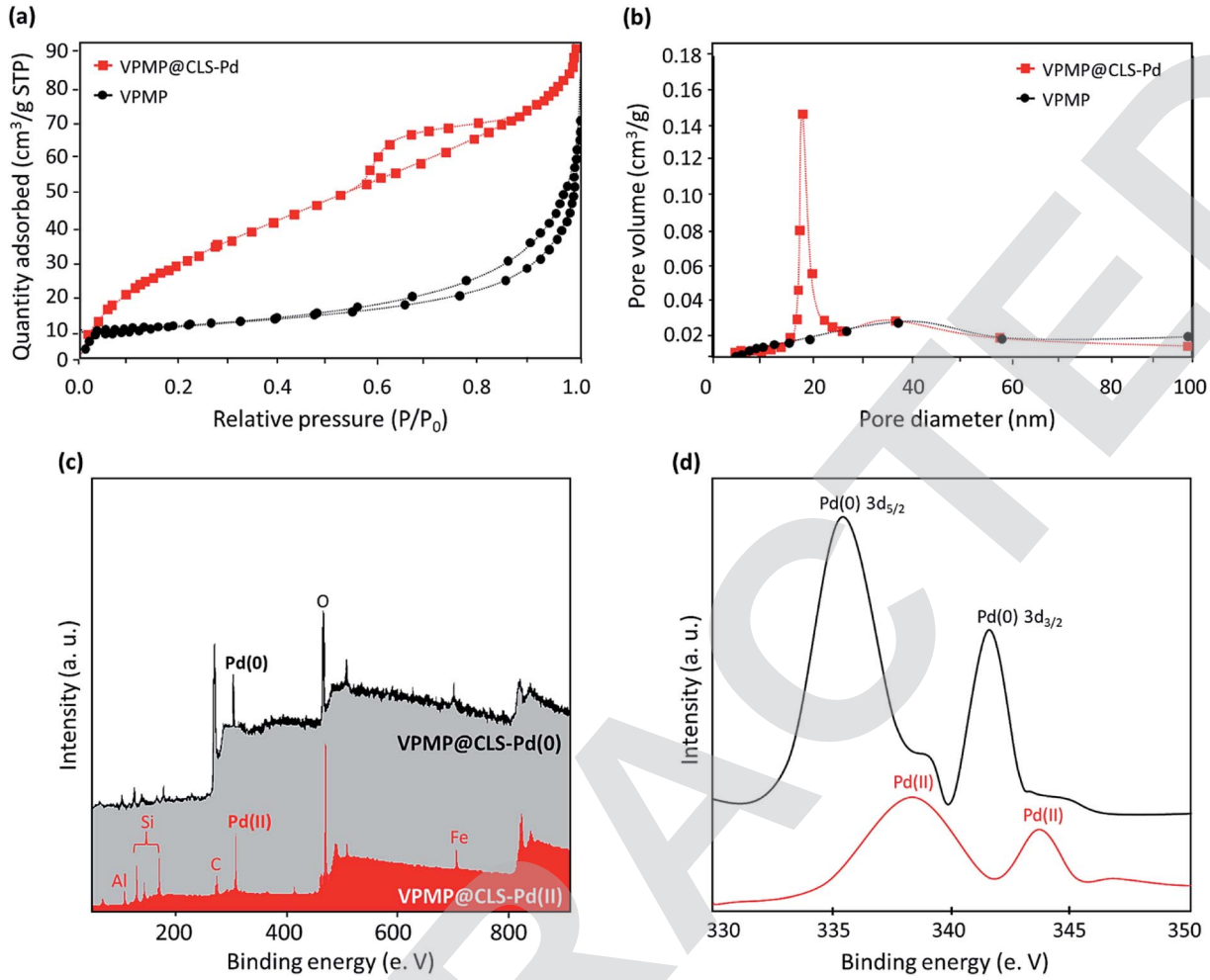

Fig. 5 (a) BET curves, and (b) pore size distribution diagram of the individual VPMP and VPMP@CLS-Pd composite, and (c and d) XPS spectra of the VPMP@CLS-Pd(II) and VPMP@CLS-Pd(0) composites.

the interior capacity of the pore sizes has been decreased after the composition of the sole VPMP with CLS and Pd NPs. In fact, it seems that a large part of the pores have been occupied by the spherical Pd NPs and CLS strands. From the curves, this is figured out that all of the pores have been filled by liquid N_2 at $P/P_0 = 0.99$, for VPMP@CLS-Pd composite. So, total pore volume of our sample can be estimated from the amount adsorbed at $P/P_0 = 0.99$ (72.2 $cm^3\ g^{-1}$ STP) and convert it to liquid volume (gas per liquid volume ratio is 647 for N_2 at 77 K), then the total pore volume is: 72.2/647 = 0.111 $cm^3\ g^{-1}$.[45] Moreover, the pore size distribution was investigated for the prepared VPMP@CLS-Pd composite *via* Barrett–Joyner–Halenda method. According to the Fig. 5(b), VPMP@CLS-Pd composite has demonstrated a very narrower mesoporous pore size distribution in a size range from 17 to 27 nm that proves mesoporosity of the prepared VPMP@CLS-Pd composite.

For the structural confirmation and proving the existence of the essential elements like Pd, EDX analysis has been done and discussed (Fig. 2(b)). Moreover, this is necessary to investigate the chemical state of the Pd NPs and verify that the reduction process of Pd(II) has been successfully performed by sodium borohydride and triphenylphosphine. For this purpose, X-ray photoelectron spectroscopy (XPS) analysis was performed. As can be seen in Fig. 5(c and d), the peaks appeared at *ca.* 338 and 344 eV for the spectrum of VPMP@CLS-Pd(II) (red color spectrum), have shifted to *ca.* 331 and 342 eV after the reduction process. This shifting in the place for the peaks related to orbitals $3d_{5/2}$ and $3d_{3/2}$ of Pd NPs coming from the successful reduction of Pd(II).[46]

2.3. Application of the prepared VPMP@CLS-Pd nanocatalyst in the synthesis of biphenyl pharmaceutical derivatives

2.3.1. Optimization. To initiate assessments on the catalytic performance of the fabricated VPMP@CLS-Pd nanocatalyst, 4-nitroiodobenzene and phenylboronic acid were chosen for carrying out the coupling reaction. A general scheme of the catalyzed synthetic reaction has been exhibited in Scheme 1. In this regard, several runs were done to investigate various conditions and finding the most appropriate catalytic ratio, temperature, medium, reaction time and *etc.* To check the coupling reaction progress thin-layer chromatography (TLC)

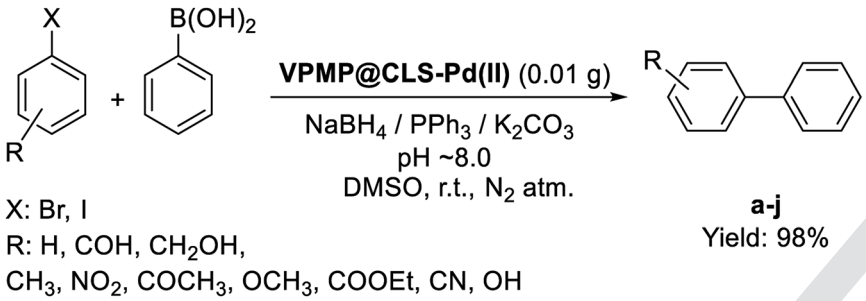

Scheme 1 General schematic of the synthetic reactions of biphenyl derivatives, catalyzed by VPMP@CLS-Pd catalytic system. The *in situ* reduction of VPMP@CLS-Pd(II) has shown more satisfying result than using the as-prepared VPMP@CLS-Pd(0) catalyst.

was used. For purification of the desired biphenyl products, flash-column chromatography (FCC) was applied. However, the obtained results have been concisely reported in Table 1, showing that the most desirable result is obtained in dimethyl sulfoxide (DMSO) using just 10 mg of VPMP@CLS-Pd catalyst particles, during 10 min stirring under mild conditions (Table 1, entry 5). As discussed in the preparation section (Section 2.1), we intended to compare the efficiency of the as-prepared

Table 2 The synthesized biphenyl derivatives from different Ar–X compounds and phenylboronic acid catalyzed by VPMP@CLS-Pd catalytic system, under optimal conditions

				Melting point (°C)		
Entry	Structure of the used Ar–X compound	Product code	Yield (%)	Observed	Reported	Ref.
1	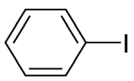	**a**	86	70	69–70	47
2	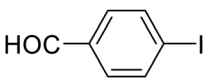	**b**	90	59–60	57–59	47
3	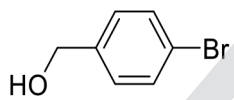	**c**	86	99–100	99	48
4	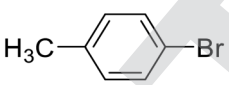	**d**	75	50–51	49–50	49
5	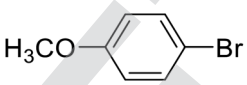	**e**	69	89–90	87–89	49
6	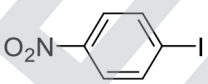	**f**	98	114–115	114	49
7	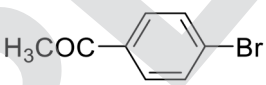	**g**	94	121	120–121	50
8	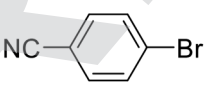	**h**	97	86–87	85–87	49
9	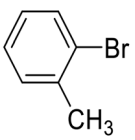	**i**	73	Liquid	—	51
10	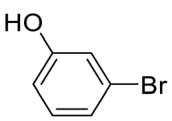	**j**	83	80	78–80	52

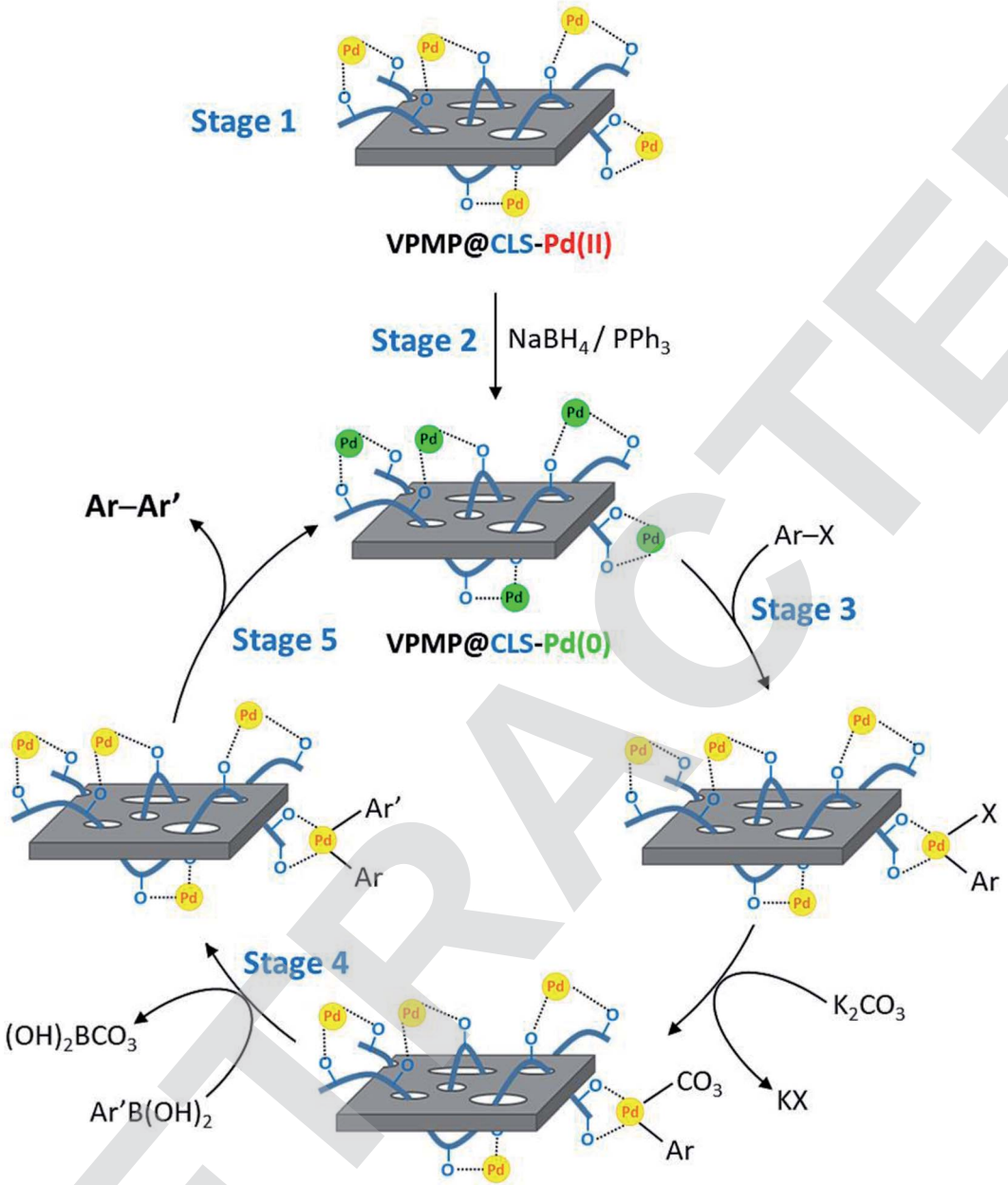

Fig. 6 Plausible mechanism for the synthesis of biphenyl derivatives, catalyzed by VPMP@CLS-Pd catalytic system.

VPMP@CLS-Pd(0) catalyst with the freshly reduced VPMP@CLS-Pd(II) version, in the coupling reaction. As can be observed in the Table 1 (entries 5 and 6), a noticeable difference is observed between these two attitudes. A probable justification for this observation has been submitted in the preparation section.

2.3.2. Synthesis of the various biphenyl derivatives. The performance of the presented catalytic system was further monitored by the synthesis of the various biphenyl derivatives. For this purpose, different derivatives of Ar–X compound were used, as listed in Table 2. As can be observed, high reaction yields have been obtained for the majority of the synthesized products in the presence of VPMP@CLS-Pd catalytic system. It should be noted that all of the reactions have been carried out in the determined optimal conditions (in previous section), and TLC and FCC methods were used for screening the reaction progress and purification of the products, respectively. For identification of the synthesized biphenyl products, melting point measurement and nuclear magnetic resonance (NMR) spectroscopic methods were applied. The original ^{1}H NMR spectra of all the produced biphenyl derivatives have been given in ESI file (Fig. S1–S10†).

2.3.3. Suggested mechanism. Fig. 6 schematically presents the suggested mechanism for the catalytic role of the fabricated VPMP@CLS-Pd catalytic system, in the synthetic reactions of biphenyl derivatives. From chemical aspect, it would be an

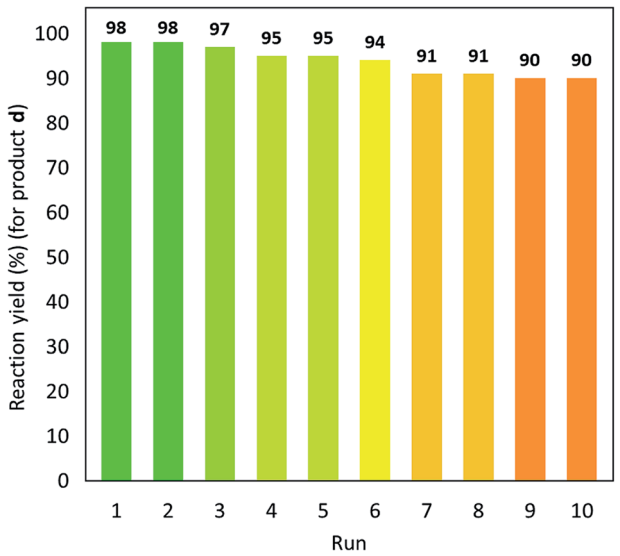

Fig. 7 Recyclability diagram of VPMP@CLS-Pd catalytic system in the synthesis reaction of product **f**.

important issue to reduce the formed Pd NPs from chemical state Pd^{2+} to Pd^0 because Pd^0 is in activated form and could be settled in the Ar–X bond.[53] As discussed in the previous sections, we compared the catalytic efficiency for both as-prepared VPMP@CLS-Pd(0) (as shown in Fig. 1), and the freshly prepared version (as shown in Fig. 6) in which VPMP@CLS-Pd(II) is added to the mixture of the coupling reaction, and Pd(II) NPs are reduced during an *in situ* process. However, this purpose is followed by using sodium borohydride in the presence of triphenylphosphine as the reducing agent and appropriate ligand for the reduced Pd, respectively. In Table 1, it has been demonstrated that it will be better to store the presented catalyst in VPMP@CLS-Pd(II) state, and perform the reduction process at the same time with the catalytic process. At this attitude, effective electronic interactions between the Pd NPs (in chemical state Pd^{2+}) and present heteroatoms in the structure of the reactants lead to more availability and probability to collision between the involved molecules in the reaction. So, in summary: stage (1) effective electronic interactions cause molecules to be approached to each other by Pd^{2+}, stage (2) Pd^{2+} is reduced to Pd^0 by sodium borohydride and triphenylphosphine, stage (3) Ar–X bond is activated by Pd NPs, stage (4) Ar' (coming from $Ar'B(OH)_2$) is attached to Pd NPs, stage (5) a reductive elimination is occurred and desired biphenyl compound is formed.

2.3.4. Recyclability. Reusability of the fabricated VPMP@CLS-Pd catalytic system was also monitored by running of the catalytic process for the successive 10 times. For this purpose, coupling of 4-nitroiodobenzene and phenylboronic acid (product **f**) was considered as the pilot reaction. As Fig. 7 demonstrates, no significant change is observed in the reaction yield after 10 times recycling the catalyst and applying again. It should be noted that recycling process is conveniently carried out using *via* collecting the particles by an external magnet, washing, and drying.

2.3.5. Brief comparison with other similar systems. According to the literature, turnover frequency (TOF), as a determinative criterion for the efficiency of the Pd-based catalytic systems, is reduced proportional to increase in the size of palladium particles in Suzuki–Miyaura coupling reaction.[54] In another valid report, it has been claimed that Pd^0 clusters with the size of *ca.* 80 nm are formed from the Pd particles with *ca.* 9 nm diameter, during the reduction process.[55] In this work, Fig. 4(d) has clearly illustrated and confirmed the formation of Pd nanoparticles in a size range from 5 nm (in dispersed form) to >100 nm diameter (in agglomerated form). As the main reason for the observed extreme agglomeration of the particles, existence of the CLS matrix can be referred, since the CLS strands are able to create sticky textures in the composite. However, since the size of Pd nanoparticles in our study has exceeded 100 nm in the cluster form, it is necessary to make a brief comparison in catalytic efficiency between the present work and other previously reported systems. As can be observed in Table 3 (entry 5), great catalytic efficiency has been observed for VPMP@CLS-Pd system, during a shorter reaction time especially in comparison with entry 2, in which almost similar Pd nanoparticles (in size) have been used. This noticeable upshot can be attributed to the mesoporous structure of VPMP that provides suitable substrate for capturing the reactants and creation of the effective electronic interactions in the voids.

3. Experimental

3.1. Materials and equipment

All of the applied materials and equipment have been listed in Table S1, in ESI file.†

Table 3 A brief comparison between the presented catalytic system in this work and other previously reported systems, which included Pd nanoparticles

Entry	Catalyst	Pd particle size (nm)	Catalyst (mol%)	Time (min)	Yield (%)	Ref.
1	PVP-stabilized Pd[a]	1.8	0.03	80	60	54
2	GO–Pd[b]	80	1.00	1440	70	55
3	MIL-53(Al)–NH_2–Pd[c]	10	0.50	30	97	56
4	Pd/Fe_3O_4	15	0.20	60	96	57
5	VPMP@CLS-Pd[d]	89	0.33[e]	10	98	—

[a] PVP: polyvinylpyrrolidone. [b] GO: graphene oxide. [c] MIL-53: is a metal–organic framework including H_2N-BDC: 2-aminoterephthalic acid (MIL stands for materials of Institut Lavoisier). [d] The present work. [e] Calculations have been submitted in ESI file.

3.2. Methods

3.2.1. Preparation of VPMP micro-plates. The purchased pumice powder (5.0 g) was placed into the milling bowl and grinded *via* ball-milling (50 Hz), for 1 h. Then, the grinded pumice was transferred to a crucible (50 mL) and the calcination process was carried out at 400 °C, for 6 h. After completion of the calcination process and cooling down to room temperature, 2.0 g of the pumice was placed into a glass round bottom flask (50 mL) and dispersed in the as-prepared HCl solution (0.1 M, 20 mL) *via* ultrasonication by using a cleaner bath (30 KHz, 200 W L^{-1}), at room temperature. Next, the mixture was stirred for 12 h at the same conditions. Ultimately, the VPMP particles were magnetically collected and washed with deionized water for several times, and then dried in oven (60 °C) for 24 h.

3.2.2. Preparation of VPMP@CLS composite. In a glass round bottom flask (100 mL), 0.01 g of CLS powder was placed and deionized water (20 mL) was added and well mixed *via* stirring at room temperature until a clear colorless solution was obtained. Afterward, VPMP (1.0 g) was added and dispersed, and then stirring was continued for 6 h, under the same conditions. After completion, the prepared magnetic VPMP@CLS particles were collected, washed with deionized water, and dried (as explained in the previous section).

3.2.3. Preparation of VPMP@CLS-Pd(II) composite

3.2.3.1 Solution A. A solution of $PdCl_2$ (0.1 M, in HCl solution) was prepared. For this purpose, in a glass round bottom flask (25 mL), brown powder of $PdCl_2$ salt was dissolved in deionized water that was heated to around 60 °C, and the pH value was reduced to ~3 by addition of two drops (0.1 mL) of the concentrate HCl. After forming a red clear solution, it was cooled down to room temperature.

3.2.3.2 Mixture A. In a glass round bottom flask (100 mL), VPMP@CLS particles (0.5 g) were dispersed in deionized water (10 mL) *via* ultrasonication, and the as-prepared solution of KOH (1.0 M, 2.0 mL) was added drop by drop, during the ultrasonication at room temperature.

Finally, solution A was dropwise added to the content of mixture A, during the stirring at room temperature. After completion of the addition, the mixture was stirred for additional 12 h, at the same conditions. Separation and purification was carried out as explained at the end of the previous sections.

3.2.4. Preparation of VPMP@CLS-Pd(0) composite. In a round bottom flask (50 mL), VPMP@CLS-Pd(II) particles (0.1 g) was placed and dispersed in DMSO (5.0 mL) *via* ultrasonication. Then, the pH of the mixture was tuned at *ca.* 8.0 by addition of K_2CO_3 (0.4 g). Next, $NaBH_4$ (0.05 g, 1.0 mmol) and PPh_3 (0.026 g, 1.0 mmol) were added into the flask and the mixture was stirred for 30 min, under N_2 atmosphere at room temperature. Finally, the particles were magnetically separated, washed and dried in a vacuum oven.

3.2.5. General procedure for the synthesis of biphenyl derivatives by VPMP@CLS-Pd catalytic system (*in situ* reduction of Pd^{2+}). In a round bottom flask (100 mL), the VPMP@CLS-Pd(II) particles (0.01) were dispersed in DMSO (5.0 mL) *via* ultrasonication, at room temperature. Then, aryl halide (1.0 mmol), phenylboronic acid (1.2 mmol), $NaBH_4$ (0.005 g, 0.1 mmol), K_2CO_3 (0.21 g, 1.5 mmol) and PPh_3 (0.0026 g, 0.1 mmol) were added into the flask and the mixture was stirred for appropriate time, under N_2 atmosphere. After completion of the reaction, catalyst was magnetically separated and the desired product was purified *via* FCC method.

3.2.6. Spectral data

*Biphenyl (**a**).* ^{1}H NMR (500 MHz, DMSO, δ, ppm): 7.34 (2H, t, J = 7.4 Hz, H-Ar), 7.44 (4H, t, J = 7.8 Hz, H-Ar), 7.62 (4H, d, J = 7.3 Hz, H-Ar).

*4-Carbaldehyde-biphenyl (**b**).* ^{1}H NMR (500 MHz, DMSO, δ, ppm): 7.40–7.52 (3H, m, H-Ar), 7.75 (2H, d, J = 7.6 Hz, H-Ar), 7.86 (2H, d, J = 6.8 Hz, H-Ar), 7.98 (2H, d, J = 6.8 Hz, H-Ar), 10.05 (1H, s, CHO).

*4-Methanol-biphenyl (**c**).* ^{1}H NMR (500 MHz, DMSO, δ, ppm): 4.54 (2H, d, J = 9.4 Hz, CH_2), 5.24 (H, t, J = 9.5 Hz, OH), 7.31–7046 (5H, m, H-Ar), 7.59–7.65 (4H, m, H-Ar).

*4-Methyl-biphenyl (**d**).* ^{1}H NMR (500 MHz, $CDCl_3$, TMS): δ 7.58 (d, 2H, J = 7.5 Hz), 7.49 (d, 2H, J = 8.0 Hz), 7.43 (t, 2H, J = 7.5 Hz), 7.32 (t, 1H, J = 7.3 Hz), 7.25 (d, 2H, J = 7.5 Hz).

*4-Methoxy-biphenyl (**e**).* ^{1}H NMR (500 MHz, $CDCl_3$, TMS): δ 7.54 (q, 4H, J = 6.7 Hz), 7.42 (t, 2H, J = 7.7 Hz), 7.28 (t, 1H, J = 14.8 Hz), 6.98 (d, 2H, J = 4.3 Hz), 3.86 (s, 3H).

*4-Nitro-biphenyl (**f**).* ^{1}H NMR (500 MHz, $CDCl_3$, TMS): δ 8.32 (d, 2H, J = 9.0 Hz), 7.75 (d, 2H, J = 9.0 Hz), 7.64 (d, 2H, J = 7.0 Hz), 7.51 (t, 2H, J = 7.5 Hz), 7.46 (t, 1H, J = 7.2 Hz).

*1-Biphenyl-4-yl-ethanone (**g**).* ^{1}H NMR (500 MHz, $CDCl_3$, TMS): δ 8.03 (d, 2H, J = 8.4 Hz), 7.69 (d, 2H, J = 4.0 Hz), 7.63 (t, 2H, J = 4.5 Hz), 7.48 (t, 2H, J = 7.5 Hz), 7.40 (t, 1H, J = 7.0 Hz), 2.64 (s, 3H).

*Biphenyl-4-carbonitrile (**h**).* ^{1}H NMR (500 MHz, $CDCl_3$, TMS): δ 7.73 (d, 2H, J = 8.5 Hz), 7.68 (d, 2H, J = 8.5 Hz), 7.59 (t, 2H, J = 4.5 Hz), 7.48 (t, 2H, J = 7.5 Hz), 7.42 (m, 1H).

*2-Methyl-biphenyl (**i**).* ^{1}H NMR (500 MHz, $CDCl_3$, TMS): δ 7.42 (t, 2H, J = 7.5 Hz), 7.34 (m, 3H), 7.26 (m, 4H), 2.28 (s, 3H).

*Biphenyl-3-ol (**j**).* ^{1}H NMR (500 MHz, $CDCl_3$, TMS): δ 7.56 (d, 2H, J = 7.7 Hz), 7.43 (t, 2H, J = 7.6 Hz), 7.34 (m, 2H), 7.17 (d, 1H, J = 7.7 Hz), 7.06 (s, 1H), 6.82 (m, 1H), 4.82 (s, 1H).

4. Conclusion

An efficient heterogeneous catalytic system based on the principles of green chemistry has been presented and suitably applied in the synthetic reactions of biphenyl pharmaceutical compounds. In summary, volcanic pumice magnetic particles (VPMP) in micro scale have been constructively composed with cellulose (CLS) natural polymeric strands. Briefly, two aims were pursued by this composition: (first) inherent magnetic property of VPMP that provides a great possibility to isolate the catalyst particles with high convenience, (second) high heterogeneity and structural stability is obtained by the VPMP that results in significant recyclability for the catalyst. Moreover, palladium nanoparticles (Pd NPs) have been incorporated to the structure as the main catalytic sites. For the synthetic reactions of the biphenyl pharmaceutical derivatives (*via* Suzuki approach), the present Pd(II) NPs onto the surfaces were reduced to Pd(0). In this regard, a plausible mechanism has been suggested in the

context, as well. However, all of the essential analyses such as FT-IR, EDX, VSM, TGA, FESEM and TEM, BTE, and XPS, have been performed for characterization of the fabricated VPMP@CLS-Pd composite. From the obtained results, it was revealed that all three ingredients have been constructively composed with each other. Also, as the main upshot it was found out that the spherical-shaped nanoscale Pd particles (in chemical state Pd^0) have been well distributed onto the surfaces of the porous laminate-shaped of VPMP. Ultimately, the novel designed VPMP@CLS-Pd catalyst was used for facilitating the synthetic reactions of biphenyls, and it was observed that high reaction yields (~98%) are obtained in a short reaction time (10 min), through using a small amount of catalytic system (0.01 g) under mild reaction conditions (room temperature). Overall, due to taking advantage from natural components in the structure of the VPMP@CLS-Pd, high catalytic performance, and great reusability, the novel presented system is strongly recommended for scaling up and industrial applications.

Conflicts of interest

Authors declare no conflict of interest.

Acknowledgements

The authors gratefully acknowledge the partial support from the Research Council of University of Tehran (UT) and also Iran University of Science and Technology (IUST).

References

1 X. Xue, Z. Zhaoa and Y. Wang, Retraction: a miraculous chiral Ir–Rh bimetallic nanocatalyst for asymmetric hydrogenation of activated ketones, *Org. Chem. Front.*, 2019, **6**, 3603.

2 Y. Qiu, Y. Zhang, L. Jin, L. Pan, G. Du, D. Ye and D. Wang, Immobilization of manganese dioxide nanoparticles on modified poly 2,4-dichlorostyrene microspheres: a highly efficient and recyclable catalyst for borrowing hydrogen reactions, *Org. Chem. Front.*, 2019, **6**, 3420–3427.

3 G. Bao, J. Bai and C. Li, Synergistic effect of the Pd–Ni bimetal/carbon nanofiber composite catalyst in Suzuki coupling reaction, *Org. Chem. Front.*, 2019, **6**, 352–361.

4 M. B. Gawande, Y. Monga, R. Zboril and R. K. Sharma, Silica-decorated magnetic nanocomposites for catalytic applications, *Coord. Chem. Rev.*, 2015, **288**, 118–143.

5 A. Maleki, R. Taheri-Ledari and M. Soroushnejad, Surface functionalization of magnetic nanoparticles *via* palladium-catalyzed Diels-Alder approach, *ChemistrySelect*, 2018, **3**, 13057–13062.

6 A. Maleki, R. Taheri-Ledari, J. Rahimi, M. Soroushnejad and Z. Hajizadeh, Facile peptide bond formation: Effective interplay between isothiazolone rings and silanol groups at silver/iron oxide nanocomposite surfaces, *ACS Omega*, 2019, **4**, 10629–10639.

7 A. Maleki, M. Niksefat, J. Rahimi and R. Taheri-Ledari, Multicomponent synthesis of pyrano[2,3-d]pyrimidine derivatives *via* a direct one-pot strategy executed by novel designed copperated Fe_3O_4@polyvinyl alcohol magnetic nanoparticles, *Mater. Today Chem.*, 2019, **13**, 110–120.

8 R. Taheri-Ledari, J. Rahimi and A. Maleki, Synergistic catalytic effect between ultrasound waves and pyrimidine-2,4-diamine-functionalized magnetic nanoparticles: applied for synthesis of 1,4-dihydropyridine pharmaceutical derivatives, *Ultrason. Sonochem.*, 2019, **59**, 104737.

9 R. Taheri-Ledari, K. Valadi, S. Gharibi and A. Maleki, Synergistic photocatalytic effect between green LED light and Fe_3O_4/ZnO-modified natural pumice: a novel cleaner product for degradation of methylene blue, *Mater. Res. Bull.*, 2020, **130**, 110946.

10 W. Zhang, R. Taheri-Ledari, Z. Hajizadeh, E. Zolfaghari, M. R. Ahghari, A. Maleki, M. R. Hamblin and Y. Tian, Enhanced activity of vancomycin by encapsulation in hybrid magnetic nanoparticles conjugated to a cell-penetrating peptide, *Nanoscale*, 2020, **12**, 3855–3870.

11 R. Taheri-Ledari, J. Rahimi and A. Maleki, Method screening for conjugation of the small molecules onto the vinyl-coated Fe_3O_4/silica nanoparticles: highlighting the efficiency of ultrasonication, *Mater. Res. Express*, 2020, **7**, 015067.

12 R. Eyvazzadeh-Keihan, N. Bahrami, R. Taheri-Ledari and A. Maleki, Highly facilitated synthesis of phenyl(tetramethyl)acridinedione pharmaceuticals by a magnetized nanoscale catalytic system, constructed of GO, Fe_3O_4 and creatine, *Diamond Relat. Mater.*, 2020, **102**, 107661.

13 S. Kapoor, V. Kumar, K. B. Tikoo, B. Chudasama, N. Goel and S. Singhal, Strategically designed reduced graphene oxide based magnetic responsive nanocatalysts for the attenuation of recalcitrant pollutants, *Ceram. Int.*, 2020, **46**, 2724–2742.

14 Z. Hajizadeh, K. Valadi, R. Taheri-Ledari and A. Maleki, Convenient Cr(VI) removal from aqueous samples: executed by a promising clay-based catalytic system, magnetized by Fe_3O_4 nanoparticles and functionalized with humic acid, *ChemistrySelect*, 2020, **5**, 2441–2448.

15 M. Hamidinasab, M. A. Bodaghifard and A. Mobinikhaledi, Green synthesis of 1*H*-pyrazolo[1,2-*b*] phthalazine-2-carbonitrile derivatives using a new bifunctional base-ionic liquid hybrid magnetic nanocatalyst, *Appl. Organomet. Chem.*, 2020, **34**, 5386.

16 J. Rahimi, R. Taheri-Ledari, M. Niksefat and A. Maleki, Enhanced reduction of nitrobenzene derivatives: effective strategy executed by Fe_3O_4/PVA-10% Ag as a versatile hybrid nanocatalyst, *Catal. Commun.*, 2020, **134**, 105850.

17 S. Parvaz, R. Taheri-Ledari, M. S. Esmaeili, M. Rabbani and A. Maleki, A brief survey on the advanced brain drug administration by nanoscale carriers: with a particular focus on AChE reactivators, *Life Sci.*, 2020, **240**, 117099.

18 R. Taheri-Ledari, A. Maleki, E. Zolfaghari, M. Radmanesh, H. Rabbani, A. Salimi and R. Fazel, High-performance sono/nano-catalytic system: Fe_3O_4@Pd/$CaCO_3$-DTT core/shell nanostructures, a suitable alternative for traditional reducing agents for antibodies, *Ultrason. Sonochem.*, 2020, **61**, 104824.

19 R. Taheri-Ledari, S. M. Hashemi and A. Maleki, High-performance sono/nano-catalytic system: CTSN/Fe_3O_4–Cu nanocomposite, a promising heterogeneous catalyst for the synthesis of N-arylimidazoles, *RSC Adv.*, 2019, **9**, 40348–40356.

20 M. M. Ayad, W. A. Amer and M. G. Kotp, Magnetic polyaniline-chitosan nanocomposite decorated with palladium nanoparticles for enhanced catalytic reduction of 4-nitrophenol, *Mol. Catal.*, 2017, **439**, 72–80.

21 S. S. Soltani, M. Golshani, S. Moghimi, S. M. Farnia, S. Ketabforoush, T. Akbarzadeh and A. Foroumadi, Green decarboxylative aminoalkylation of coumarin-3-carboxylic acids, *ChemistrySelect*, 2019, **4**, 13695–13697.

22 A. Ramu and K. Rajendrakumar, Natural catalyst mediated ARGET and SARA ATRP of N-isopropylacrylamide and methyl acrylate, *Polym. Chem.*, 2020, **11**, 687–694.

23 H. B. Hadjltaief, M. E. Galvez, M. B. Zina and P. D. Costa, TiO_2/clay as a heterogeneous catalyst in photocatalytic/photochemical oxidation of anionic reactive blue 19, *Arabian J. Chem.*, 2019, **12**, 1454–1462.

24 J. Yao, L. Shi, W. Deng, J. Fan, Y. Wang, W. Gao, D. Zhang, W. Zhub and Z. Liu, Facile sulfolane-modified resins for enhanced dimethoxymethane carbonylation, *Catal. Sci. Technol.*, 2020, **10**, 2561–2572.

25 T. Baran, Pd NPs@Fe_3O_4/chitosan/pumice hybrid beads: a highly active, magnetically retrievable, and reusable nanocatalyst for cyanation of aryl halides, *Carbohydr. Polym.*, 2020, **237**, 116105.

26 A. S. Yusuff, L. T. Popoola and E. I. Aderibigbe, Solar photocatalytic degradation of organic pollutants in textile industry wastewater by ZnO/pumice composite photocatalyst, *J. Environ. Chem. Eng.*, 2020, **8**, 103907.

27 A. Mohseni-Bandpei, A. Eslami, H. Kazemian, M. Zarrabi and T. J. Al-Musawi, A high density 3-aminopropyltriethoxysilane grafted pumice-derived silica aerogel as an efficient adsorbent for ibuprofen: characterization and optimization of the adsorption data using response surface methodology, *Environ. Technol.*, 2020, **18**, 100642.

28 K. Valadi, S. Gharibi, R. Taheri-Ledari and A. Maleki, Ultrasound-assisted synthesis of 1,4-dihydropyridine derivatives by an efficient volcanic-based hybrid nanocomposite, *Solid State Sci.*, 2020, **101**, 106141.

29 A. Maleki, S. Gharibi, K. Valadi and R. Taheri-Ledari, Pumice-modified cellulose fiber: an environmentally benign solid state hybrid catalytic system for the synthesis of 2,4,5-triarylimidazole derivatives, *J. Phys. Chem. Solids*, 2020, **142**, 109443.

30 D. Li, J. Zhang and C. Cai, Pd nanoparticles supported on cellulose as a catalyst for vanillin conversion in aqueous media, *J. Org. Chem.*, 2018, **83**, 7534–7538.

31 M. A. Khalilzadeh, S. Tajik, H. Beitollahi and R. A. Venditti, Green synthesis of magnetic nanocomposite with iron oxide deposited on cellulose nanocrystals with copper (Fe_3O_4@CNC/Cu): investigation of catalytic activity for the development of a venlafaxine electrochemical sensor, *Ind. Eng. Chem. Res.*, 2020, **59**, 4219–4228.

32 H. Zhang, T. Liu, Y. Zhu, L. Hong, T. Li, X. Wang and Y. Fu, Lipases immobilized on the modified polyporous magnetic cellulose support as an efficient and recyclable catalyst for biodiesel production from yellow horn seed oil, *Renewable Energy*, 2020, **145**, 1246–1254.

33 S. F. Hamzavi, S. Gerivani, S. Saeedi, K. Naghdipari and G. Shahverdizadeh, Preparation and characterization of a novel spherical cellulose-copper(II) oxide composite particles: as a heterogeneous catalyst for the click reaction, *Mol. Diversity*, 2020, **24**, 201–209.

34 M. Kempasiddaiah, V. Kandathil, R. B. Dateer, B. S. Sasidhar and S. A. Patil, Immobilizing biogenically synthesized palladium nanoparticles on cellulose support as a green and sustainable dip catalyst for cross-coupling reaction, *Cellulose*, 2020, **27**, 3335–3357.

35 S. S. Soltani, S. M. Farnia and A. Foroumadi, A comparison between Suzuki cross-coupling reaction and direct arylation in the synthesis of new antibacterial imidazo-pyrazines/pyridazines, *J. Heterocycl. Chem.*, 2020, **57**, 1770–1780.

36 A. Maleki, R. Taheri-Ledari and R. Ghalavand, Design and fabrication of a magnetite-based polymer-supported hybrid nanocomposite: a promising heterogeneous catalytic system utilized in known palladium-assisted coupling reactions, *Comb. Chem. High Throughput Screening*, 2020, **23**, 119–125.

37 D. Gala, A. Stamford, J. Jenkins and M. Kugelman, One-step synthesis of ciphenylacetic acids *via* Pd/C-catalyzed arylation, *Org. Process Res. Dev.*, 1997, **1**, 163–164.

38 A. Sharma, B. Chakravarti, M. P. Gupt, J. A. Siddiqui, R. Konwar and R. P. Tripathi, Synthesis and anti-breast cancer activity of biphenyl based chalcones, *Bioorg. Med. Chem.*, 2010, **18**, 4711–4720.

39 J. T. Perkins, M. C. Petriello, B. J. Newsome and B. Hennig, Polychlorinated biphenyls and links to cardiovascular disease, *Environ. Sci. Pollut. Res. Int.*, 2016, **23**, 2160–2172.

40 J. V. Bruckner, K. L. Khanna and H. H. Cornish, Polychlorinated biphenyl-induced alteration of biologic parameters in the rat, *Toxicol. Appl. Pharmacol.*, 1974, **28**, 189–199.

41 K. Thapa, P. Paul and S. Bhattacharya, A group of diphosphine-thiosemicarbazone complexes of palladium: efficient precursors for catalytic CC and CN coupling reactions, *Inorg. Chim. Acta*, 2019, **486**, 232–239.

42 Z. Chen, E. Vorobyeva, S. Mitchell, E. Fako, M. A. Ortuño, N. López, S. M. Collins, P. A. Midgley, S. Richard, G. Vilé and J. Pérez-Ramírez, A heterogeneous single-atom palladium catalyst surpassing homogeneous systems for Suzuki coupling, *Nat. Nanotechnol.*, 2018, **13**, 702–707.

43 J. Cui, N. Zhu, N. Kang, C. Ha, C. Shi and P. Wu, Biorecovery mechanism of palladium as nanoparticles by Enterococcus faecalis: from biosorption to bioreduction, *Chem. Eng. J.*, 2017, **328**, 1051–1057.

44 S. Kayal and R. V. Ramanujan, Doxorubicin loaded PVA coated iron oxide nanoparticles for targeted drug delivery, *Mater. Sci. Eng., C*, 2010, **30**, 484–490.

45 J. J. Freeman and A. I. McLeod, Nitrogen BET surface area measurement as a fingerprint method for the estimation of pore volume in active carbons, *Fuel*, 1983, **62**, 1090–1091.
46 A. B. Yousaf, M. Imran, M. Farooq and P. Kasak, Interfacial phenomenon and nanostructural enhancements in palladium loaded lanthanum hydroxide nanorods for heterogeneous catalytic applications, *Sci. Rep.*, 2018, **8**, 4354.
47 H. M. Savanur, R. G. Kalkhambkar and K. K. Laali, $Pd(OAc)_2$ catalyzed homocoupling of arenediazonium salts in ionic liquids: synthesis of symmetrical biaryls, *Tetrahedron Lett.*, 2016, **57**, 663–667.
48 R. Fareghi-Alamdari, M. Golestanzadeh and O. Bagheri, Meso-tetrakis[4-(methoxycarbonyl)phenyl] porphyrinatopalladium(II) supported on graphene oxide nanosheets (Pd(II)-TMCPP-GO): synthesis and catalytic activity, *RSC Adv.*, 2016, **6**, 108755–108767.
49 B. Tao and D. W. Boykin, Simple amine/$Pd(OAc)_2$-catalyzed Suzuki coupling reactions of aryl bromides under mild aerobic conditions, *J. Org. Chem.*, 2004, **69**, 4330–4335.
50 Y. M. A. Yamada, K. Takeda, H. Takahashi and S. Ikegami, An assembled complex of palladium and non-cross-linked amphiphilic polymer: a highly active and recyclable catalyst for the Suzuki–Miyaura reaction, *Org. Lett.*, 2002, **4**, 3371–3374.
51 N. E. Leadbeater and M. Marco, Ligand-free palladium catalysis of the Suzuki reaction in water using microwave heating, *Org. Lett.*, 2002, **4**, 2973–2976.
52 H. Sakurai, T. Tsukuda and T. J. Hirao, Pd/C as a reusable catalyst for the coupling reaction of halophenols and arylboronic acids in aqueous media, *J. Org. Chem.*, 2002, **67**, 2721–2722.
53 A. Maleki, R. Taheri-Ledari, R. Ghalavand and R. Firouzi-Haji, Palladium-decorated *o*-phenylenediamine-functionalized Fe_3O_4/SiO_2 magnetic nanoparticles: a promising solid-state catalytic system used for Suzuki–Miyaura coupling reactions, *J. Phys. Chem. Solids*, 2020, **136**, 109200.
54 P. J. Ellis, I. J. S. Fairlamb, S. F. J. Hackett, K. Wilson and A. F. Lee, Evidence for the surface-catalyzed Suzuki–Miyaura reaction over palladium nanoparticles: an operando XAS study, *Angew. Chem., Int. Ed.*, 2010, **49**, 1820–1824.
55 G. M. Scheuermann, L. Rumi, P. Steurer, W. Bannwarth and R. Mulhaupt, Palladium nanoparticles on graphite oxide and its functionalized graphene derivatives as highly active catalysts for the Suzuki–Miyaura coupling reaction, *J. Am. Chem. Soc.*, 2009, **131**, 8262–8270.
56 Y. Huang, Z. Zheng, T. Liu, J. Lü, Z. Lin, H. Li and R. Cao, Palladium nanoparticles supported on amino functionalized metal–organic frameworks as highly active catalysts for the Suzuki–Miyaura cross-coupling reaction, *Catal. Commun.*, 2011, **14**, 27–31.
57 S. Hemmati, M. Yousefi, M. Hashemi Salehi, M. Amiri and M. Hekmati, Palladium nanoparticles immobilized over Strawberry fruit extract coated Fe_3O_4 NPs: a magnetic reusable nanocatalyst for Suzuki–Miyaura coupling reactions, *Appl. Organomet. Chem.*, 2020, e5653.